Geochemistry Geophysics Geosystems G3

Article
Volume 13, Number 8
16 August 2012
Q08007, doi:10.1029/2012GC004260
ISSN: 1525-2027

Published by AGU and the Geochemical Society

Heat flow in the Lesser Antilles island arc and adjacent back arc Grenada basin

Michael Manga
Department of Earth and Planetary Science, University of California, Berkeley, California 94720, USA (manga@seismo.berkeley.edu)

Matthew J. Hornbach
Department of Earth Sciences, Southern Methodist University, Dallas, Texas 75275, USA (mhornbach@smu.edu)

Anne Le Friant
Institut de Physique du Globe de Paris, Sorbonne Paris Cite, Universite Paris Diderot, UMR 7175, CNRS, 1, rue Jussieu, FR-75238 Paris, France (lefriant@ipgp.fr)

Osamu Ishizuka
Geological Survey of Japan, AIST, Central 7 1-1-1 Higashi, Tsukuba, Ibaraki 305-8567, Japan (o-ishizuka@aist.go.jp)

Nicole Stroncik
Integrated Ocean Drilling Program, Texas A&M University, College Station, Texas 77845, USA (stroncik@iodp.tamu.edu)

Tatsuya Adachi
Graduate School of Science and Engineering, Yamagata University, Kojirakawa-machi 1-4-12, Yamagata 990-8560, Japan (s11e501m@st.yamagata-u.ac.jp)

Mohammed Aljahdali
Earth, Ocean and Atmospheric Sciences, Florida State University, Tallahassee, Florida 32306, USA (ma10u@my.fsu.edu)

Georges Boudon
Institut de Physique du Globe de Paris, Sorbonne Paris Cite, Universite Paris Diderot, UMR 7175, CNRS, 1, rue Jussieu, FR-75238 Paris, France (boudon@ipgp.fr)

Christoph Breitkreuz
Department of Geology and Paleontology, TU Bergakademie Freiberg, DE-09599 Freiberg, Germany (christoph.breitkreuz@geo.tu-freiberg.de)

Andrew Fraass
Department of Geosciences, University of Massachusetts Amherst, Amherst, Massachusetts 01003, USA (afraass@geo.umass.edu)

Akihiko Fujinawa
Department of Environmental Sciences, Ibaraki University, 2-1-1, Bunkyo, Mito 3108512, Japan (fujinawa@mx.ibaraki.ac.jp)

Robert Hatfield
CEOAS, Oregon State University, Corvallis, Oregon 97330, USA (rhatfield@coas.oregonstate.edu)

Martin Jutzeler
Geology Department, University of Otago, PO Box 56, Dunedin 9054, New Zealand (jutzeler@gmail.com)

Kyoko Kataoka
Research Institute for Natural Hazards and Disaster Recovery, Niigata University, Ikarashi 2-cho 8050, Niigata 950-2181, Japan (kataoka@gs.niigata-u.ac.jp)

Sara Lafuerza
Institut de Physique du Globe de Paris, Sorbonne Paris Cite, Universite Paris Diderot, UMR 7175, CNRS, 1, rue Jussieu, FR-75238 Paris, France (sara.lafuerz@gmail.com)

Fukashi Maeno
Volcano Research Center, Earthquake Research Institute, University of Tokyo, Tokyo 113-0032, Japan (fmaeno@eri.u-tokyo.ac.jp)

Michael Martinez-Colon
College of Marine Science, University of South Florida, St. Petersburg, Florida 33701, USA (mmartin8@mail.usf.edu)

Molly McCanta
Geology Department, Tufts University, Medford, Massachusetts 02155, USA (molly.mccanta@tufts.edu)

Sally Morgan
Department of Geology, University of Leicester, Leicester LE1 7RH, UK (sm509@le.ac.uk)

Martin R. Palmer
School of Ocean and Earth Science, University of Southampton, Southampton SO14 3ZH, UK (m.palmer@noc.soton.ac.uk)

Takeshi Saito
International Young Researchers Empowerment Center, Shinshu University, Asahi 3-1-1, Matsumoto 390-8621, Japan (saito@shinshu-u.ac.jp)

Angela Slagle
Borehole Research Group, Lamont-Doherty Earth Observatory, Earth Institute at Columbia University, 61 Route 9W, Palisades, New York 10964, USA (aslagle@ldeo.columbia.edu)

Adam J. Stinton
Montserrat Volcano Observatory, Flemmings, Montserrat (adam@mvo.ms)

Seismic Research Center, University of the West Indies, St. Augustine, Trinidad and Tobago

K. S. V. Subramanyam
Geochemistry Division, National Geophysical Research Institute, Uppal Road, Hyderabad 500 606, India (konduri2003@yahoo.com)

Yoshihiko Tamura
Institute for Research on Earth Evolution, JAMSTEC, 2-15 Natsushima-Cho, Yokosuka, Kanagawa 237-0061, Japan (tamuray@jamstec.go.jp)

Peter J. Talling
National Oceanography Center, Southampton, University of Southampton, Southampton S014 3ZH, UK (peter.talling@noc.ac.uk)

Benoit Villemant
Laboratoire de Petrologie, Geochimie, Volcanologie, University Pierre et Marie Curie–Paris 6, UMR 7193, ISTEP, 4 place Jussieu, FR-75005 Paris, France (benoit.villemant@upmc.fr)

Deborah Wall-Palmer
School of Geography, Earth and Environmental Sciences, Plymouth University, Plymouth PL4 8AA, UK (deborah.wall-palmer@plymouth.ac.uk)

Fei Wang
Institute of Geology and Geophysics, Chinese Academy of Sciences, Beijing 100029, China (wangfei@mail.iggcas.ac.cn)

[1] Using temperature gradients measured in 10 holes at 6 sites, we generate the first high fidelity heat flow measurements from Integrated Ocean Drilling Program drill holes across the northern and central Lesser Antilles arc and back arc Grenada basin. The implied heat flow, after correcting for bathymetry and sedimentation effects, ranges from about 0.1 W/m^2 on the crest of the arc, midway between the volcanic islands of Montserrat and Guadeloupe, to <0.07 W/m^2 at distances >15 km from the crest in the back arc direction. Combined with previous measurements, we find that the magnitude and spatial pattern of heat flow are similar to those at continental arcs. The heat flow in the Grenada basin to the west of the active arc is 0.06 W/m^2, a factor of 2 lower than that found in the previous and most recent study. There is no thermal evidence for significant shallow fluid advection at any of these sites. Present-day volcanism is confined to the region with the highest heat flow.

Components: 12,500 words, 5 figures, 4 tables.

Keywords: Grenada basin; IODP; Lesser Antilles; back arc; heat flow; volcanic arc.

Index Terms: 8130 Tectonophysics: Heat generation and transport; 8178 Tectonophysics: Tectonics and magmatism; 8413 Volcanology: Subduction zone processes (1031, 3060, 3613, 8170).

Received 29 May 2012; **Revised** 12 July 2012; **Accepted** 13 July 2012; **Published** 16 August 2012.

Manga, M., et al. (2012), Heat flow in the Lesser Antilles island arc and adjacent back arc Grenada basin, *Geochem. Geophys. Geosyst.*, *13*, Q08007, doi:10.1029/2012GC004260.

1. Introduction

[2] Heat flow in volcanic arcs provides insight into the thermal structure and rheology of the mantle wedge [*Kelemen et al.*, 2003], the three-dimensional mantle flow at subduction zones [e.g., *Schellart*, 2004; *Stegman et al.*, 2006], the time-averaged magma flux into the crust [e.g., *Rothstein and Manning*, 2003], and the eruption style and magma composition at arc volcanoes [*Zellmer*, 2009]. Heat flow, when combined with the flux of magma recorded by surface eruptions, provides one of the few constraints on the ratio of intruded to extruded magma volumes [*Ingebritsen et al.*, 1989; *White et al.*, 2006] and hence on the magmatic processes that build crust in volcanic arcs.

[3] In continental arcs, heat flow is reasonably well characterized by direct measurements of temperature gradients in deep holes. Examples include the North American Cascades [e.g., *Blackwell et al.*, 1990], Southern Mexico [*Ziagos et al.*, 1985], the South American Andes [e.g., *Springer and Forster*, 1998], and Japan [e.g., *Furukawa*, 1993]. Where individual measurements are not affected by shallow volcanic and hydrothermal processes or by groundwater flow, heat flow shows a consistent pattern. Heat flow generally increases from <0.05 W/m^2 in the fore arc to 0.09–0.15 W/m^2 over the active arc, and decreases in the back arc to <0.09 W/m^2. The width of the region with high heat flow typically extends a few tens of km from the crest of the arc, and may reflect the width of the region over which upwelling occurs in the mantle [e.g., *England and Katz*, 2010] or magma is intruded and stored within the crust [e.g., *Blackwell et al.*, 1982].

[4] In island arcs, heat flow may differ from continental arcs because the crust is often not as thick. For the Lesser Antilles arc we study here, the Moho

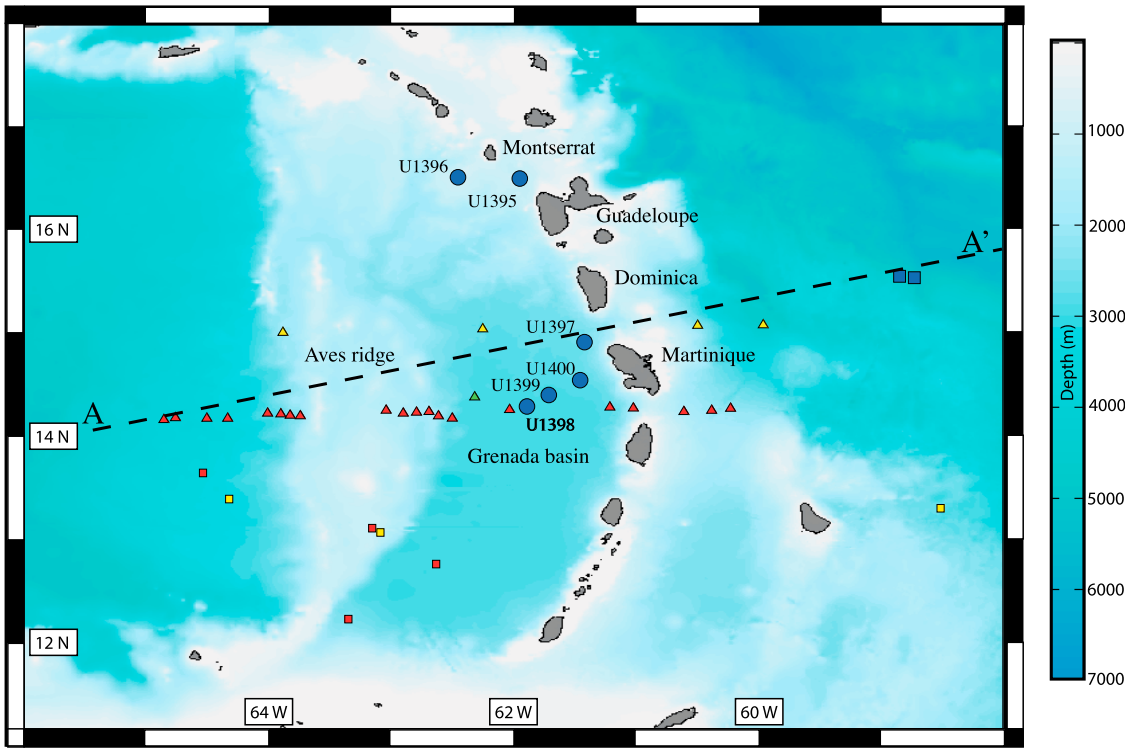

Figure 1. Lesser Antilles arc and location of heat flow measurements. Large blue disks show our new measurements. Data from previous studies: red triangles [*Clark et al.*, 1978]; yellow triangles [*Vacquier and von Herzen*, 1964]; green triangles [*Nason and Lee*, 1964]; yellow squares [*Langseth et al.*, 1966]; red squares [*Epp et al.*, 1970]; blue squares [*Fisher and Hounslow*, 1990]. The cross-section along line A-A′ is shown in Figure 4.

depth is between 24 and 34 km [*Sevilla et al.*, 2010; *Kopp et al.*, 2011]; for comparison, Moho depths are 40–50 km in the Cascades [e.g., *Porritt et al.*, 2011] and can exceed 70 km in the Andes [e.g., *Yuan et al.*, 2002]. As a consequence, melts generated in the mantle wedge, and then transported through and distilled in the crust, may have a different petrological evolution and eruptibility [*Plank and Langmuir*, 1988]. In comparison with continental arcs, measurements for island arcs are less numerous, as can be seen from data compilations [*Pollack et al.*, 1993; *Davies and Davies*, 2010] (see also International Heat Flow Commission database, available at http://www.heatflow.und.edu). In addition, most measurements of temperature are made in the upper few meters of the seafloor, which adds considerable uncertainty to the calculated heat flow from the underlying crust. Only a few island arcs have high quality heat flow measurements obtained from ocean drilling, and of these measurements, many are widely spaced, affected by fluid flow, and uncorrected for high sedimentation rates [*Sclater*, 1972; *Parson et al.*, 1992; *Lavoie et al.*, 1994].

[5] Here we report temperature measurements and calculated heat flow from 10 holes drilled at 6 sites during IODP (Integrated Ocean Drilling Program) Expedition 340 to the Lesser Antilles arc. We sampled the crest of the arc and sites extending up to 110 km away in the back-arc direction. These are the first heat flow measurements in this region in more than 30 years and the only measurements at depths greater than 15 mbsf (meters below seafloor). We find that heat flow is similar to that in continental arcs. The region with high heat flow may be confined to distances <15 km from the crest of the arc, consistent with the location of present-day volcanism. Heat flow at the crest of the arc and in the adjacent back arc basin are a factor of two lower than previous estimates [*Clark et al.*, 1978].

2. Study Site

[6] The Lesser Antilles arc (Figure 1) is an 800 km long chain of volcanic islands produced by the subduction of the South American plate beneath the Caribbean plate. Subduction rates for the past several Ma are 2–4 cm/year [*Macdonald and Holcombe*, 1978; *Minster and Jordan*, 1978]. The southern

Table 1. Properties of the 6 Sites and 10 Holes

Site	Latitude	Longitude	Water Depth	Separation of Holes	Drilled Depth Below Seafloor[a]	Sedimentation Rate
U1395	16°29.60N	61°57.08W	1201 m	one measured	281 m	90 m/Ma[b]
U1396	16°30.48N	61°27.10W	799 m	20 m	139 m	17–53 m/Ma[b,c]
U1397	14°54.41N	61°25.35W	2494 m	20 m	266 m	200 m/Ma[d]
U1398	14°16.70N	61°53.34W	2947 m	20 m	269 m	40–200 m/Ma[e]
U1399	14°23.24N	61°42.69W	2901 m	410 m	275 m	40–200 m/Ma[e]
U1400	14°32.20N	61°27.41N	2755 m	one measured	436 m	40–200 m/Ma[e]

[a]Depth of deepest hole at site.
[b]*Expedition 340 Scientists* [2012].
[c]*Le Friant et al.* [2008].
[d]*Boudon et al.* [2007].
[e]*Sigurdsson et al.* [1980] and *Reid et al.* [1996].

half of the arc, south of Martinique, consists of a single chain of islands that date to the early Eocene. To the north of Martinique, the arc is divided into two chains of islands. The islands in the eastern magmatically inactive chain are older, with thick carbonate platforms covering a volcanic basement. Tectonic adjustments during the mid-Miocene modified the orientation of the northern subducting slab, causing migration of the volcanic front to the west and the initiation of a new active arc [*Bouysse et al.*, 1990]. This western chain consists of mainly andesitic volcanic rocks younger than 20 Ma and includes all the active volcanoes [*Bouysse et al.*, 1990]. The oldest rocks dated on Montserrat, the island closest to the first drill site, are 2.6 Ma [*Harford et al.*, 2002], although volcanism of the island must have been initiated prior to its subaerial exposure. Volcanism on Martinique dates to at least 25 Ma [*Germa et al.*, 2011].

[7] To the west of the arc is the Grenada basin, now lying 3 km below sea level. It is characterized by crust thicker than 14 km and total sediment thickness may exceed 9 km [*Boynton et al.*, 1979]. 150 km west of the arc, and bounding the Grenada basin on the west, is the Aves ridge, the remnants of an older 90–60 Ma island arc [*Neill et al.*, 2011]. The inferred opening age of the Grenada basin of 60 Ma and thick crust suggest that the basin may represent stretched island arc crust [*Bouysse*, 1988] or an extended and widened forearc basin [*Aitken et al.*, 2011]. Extension of the Grenada basin ended in the Eocene [*Speed and Walker*, 1991; *Aitken et al.*, 2011].

[8] The origin and age of the crust on which the Lesser Antilles arc is forming are uncertain and possibly spatially variable. The northern part of the arc may be built on the older Aves arc whereas the southern part may be built on crust produced when the Grenada basin opened [*Speed and Walker*, 1991]. The implications of these differences for heat flow are not clear. The Grenada basin may have significantly lower heat flow than the Aves ridge at present [*Clark et al.*, 1978], though the heat flow measurements are few and are based on measurements made in the upper few meters of sediment.

[9] For the present study, temperature was measured at 6 sites, numbered U1395 through U1400. At each site, two or three holes were drilled and temperature was measured in one (Sites U1395, U1400) or two holes (all other sites). Their locations are shown in Figure 1 and attributes of each site are summarized in Table 1. These holes were drilled during IODP Expedition 340, which had the primary aims of unraveling the eruption history of the volcanoes in the Lesser Antilles arc, understanding the large debris avalanches shed from these islands, and understanding volcaniclastic sedimentation in a regional and temporal context. The holes penetrated alternating layers of hemipelagic sediment, turbidites commonly comprising volcaniclastic material, and layers of tephra formed by fallout from eruptions.

3. Methods and Measurements

[10] Downhole temperature was measured using the Advanced Piston Corer Temperature tool, 3rd generation (APCT-3). This tool allows temperature to be measured while drilling. The tool is lowered to the bottom of the coring wireline and then shot downward ~9.5 m and left in place, without fluid circulation, to record temperature. Thermal effects of drilling are minimized compared to rotary drilling. However, frictional heating still raises the probe's temperature many degrees above ambient temperature, and hence models for unsteady heat conduction must be used to interpret the raw temperature measurements. Details of the APCT-3 design, calibration, and testing are described by *Heesemann et al.*

[2006]. Deployment on Expedition 340 was the same as that described by *Heesemann et al.* [2006] for Expedition 311.

[11] Measurements were made at depths where the hole conditions were stable. The APCT-3 records temperature with a glass-encapsulated thermistor (Model YSI 55032) at the outside edge of the cutting shoe. Temperature resolution is better than 1.0 mK over the range of temperatures we measure and absolute accuracy is better than ±0.1 K [*Heesemann et al.*, 2006]. Temperature was recorded at the base of the hole for between 3 and 45 min (usually 10 min) and sampled every 2 s. While the response time of the thermistor is a couple seconds, the time for the probe's temperature and frictionally heated sediment to thermally equilibrate with their surroundings is much longer than the measurement period. Consequently, the recorded decay of temperature is fit to a theoretical solution to the temperature evolution using TP-Fit [*Fisher et al.*, 2007]. The calculated temperature depends on the thermal conductivity, density, and specific heat capacity of the surroundings. Uncertainty in these thermal properties dominates the uncertainty in the in situ pre-drilling temperature. We assume 0.9 W/mK $< k <$ 1.2 W/mK and 3.2×10^6 J/m^{3}K $< \rho C < 4.0 \times 10^6$ J/m^{3}K to calculate uncertainty, where ρC is the volumetrically averaged product of density and specific heat and k is thermal conductivity. The uncertainty on in situ temperature measurements with this approach is usually <0.06°C, and thus similar to the measurement accuracy.

[12] Thermal conductivity k was measured with a TeKa TK04 needle probe [*Blum*, 1997]. All measurements were made on whole round cores after the core equilibrated with the ambient temperature in the ship's laboratory. Only fine-grained turbidite deposits and hemipelagic sediment were measured; measurements in more coarse deposits would be affected by convection induced by the temperature gradients produced by the probe. Measurements are not corrected to in situ conditions. The effect of increasing pressure is to increase k. The pressure correction is about +1% for each 1800 m assuming a hydrostatic pressure gradient [*Ratcliffe*, 1960]. The effect of temperature is more complicated. The thermal conductivity of the solids in the matrix is inversely proportional to temperature [*Jaupart and Mareschal*, 2011]. In contrast, the thermal conductivity of water increases with temperature [*Keenan et al.*, 1978]. Corrections for pressure and temperature are smaller than the TK04 measurement uncertainty of 5%. Verification of accuracy was carried out daily with a MACOR ceramic standard.

[13] In order to interpret the temperature measurements we need to account for the effects of heat production within the marine sediments. The abundance of K, Th and U were measured in situ using the Hostile Environment Natural Gamma Ray Sonde (HNGS). The HNGS measures total and spectral gamma rays in the borehole at 20–30 cm resolution, using two bismuth germanate scintillation detectors and five-window spectroscopy to identify the concentrations of K, Th, and U. The measured values were corrected to account for the barite-weighted mud used while logging. Data are available from Sites U1395 and U1399. Sites U1396, U1398 and U1400 were not logged for operational reasons, while U1397 HNGS data were compromised by an over-sized hole diameter.

[14] Where we subsequently fit models and equations to the data, we determined model parameters and their uncertainties using the least squares Marquardt-Levenberg algorithm [*Press et al.*, 1992, chapter 15.5]. Reported uncertainties on model fits are standard errors from the regression.

4. Results

[15] Figure 2 shows temperature as a function of depth at all 6 sites. In all cases, temperature increases approximately linearly with depth. The uncertainty in the temperature gradient, assuming a linear increase in temperature, is less than 9% in all cases. The temperature gradient reported in Figure 2 is a best fit to the measurements assuming a linear variation with depth. For all the sites, we also fit the data with a quadratic function to see if there is any statistically significant curvature of temperature as a function of depth. At all sites, except Site U1398, the uncertainty in the quadratic term is greater than its value. Figure 2 shows the quadratic fit to data at Site U1398 along with the linear fit. At Site U1398, adding a quadratic term reduced the root-mean square of the residuals by 38%. The sign of the quadratic term implies upward fluid flow. There are, however, two reasons why the inference of fluid flow is uncertain at Site U1398. First, if we omit the two measurements from hole B (keeping the more numerous data from hole A and the ocean water temperature) the uncertainty in the quadratic term exceeds its value. Second, fitting the data using transdimensional Bayesian modeling [*Gallagher et al.*, 2011] shows that a linear fit is statistically favored over fits that involve additional parameters such as a quadratic fit.

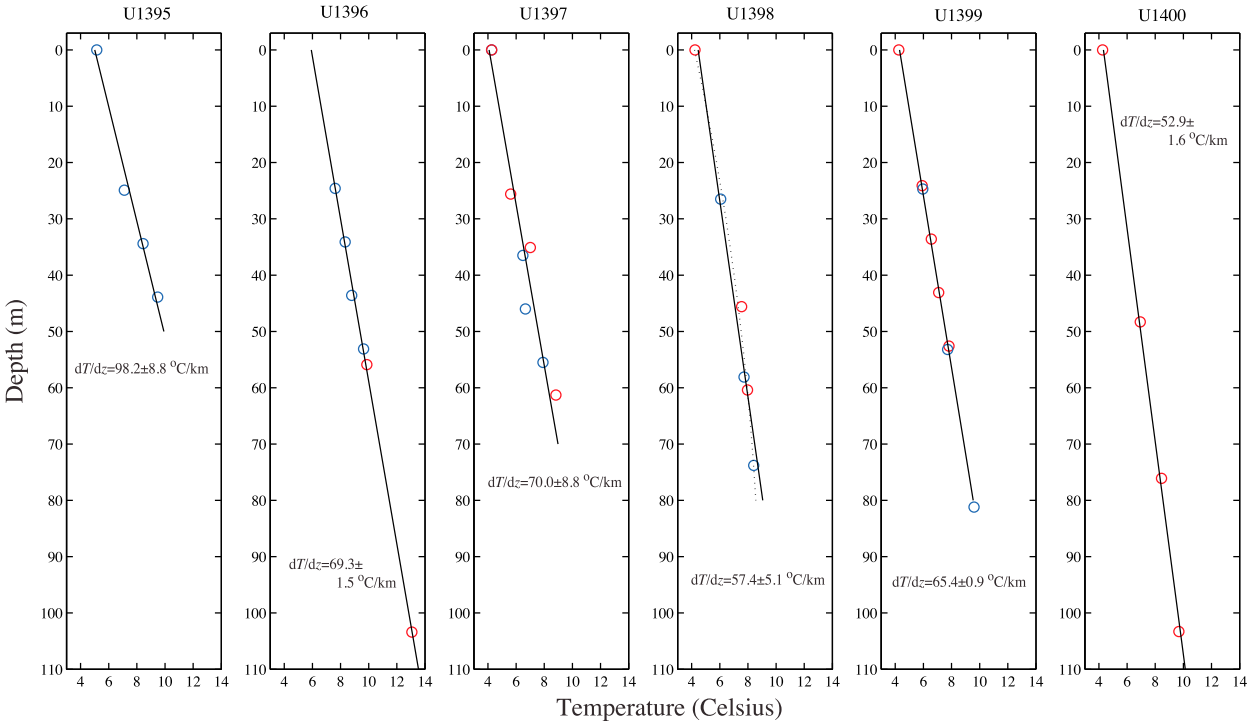

Figure 2. Temperature as a function of depth. Blue symbols indicate measurements in Hole A and red in Hole B (except U1396 where red indicates Hole C and U1400 where red indicates Hole C). At Site U1398, the best quadratic fit is shown with a dashed curve (the uncertainty on the quadratic term for all other holes is greater than its value).

[16] Figure 3 shows thermal conductivity k measured within the upper 220 m in cores recovered from all 6 sites. The mean value is 1.04 W/mK. The thermal conductivity we measure is similar to that found in other marine sediments with similar porosities and at similar depths [e.g., *Harris et al.*, 2011]. No significant changes in thermal conductivity were found over the depth range that temperature was measured: a regression between k and depth for all data shown in Figure 3 gives $dk/dz = -0.00020 \pm 0.00006$ W/m^{2}K, where z is depth. However, all sites with the exception of U1399 and U1400 have thermal conductivity statistically indistinguishable from a constant. The very weak dependence on depth is not unexpected because at all sites the porosity in the hemipelagic sediment (typically about 60%) does not change significantly over the depths that were cored, and k is inversely proportional to porosity. While porosity is expected to decrease with depth owing to compaction [*Athy*, 1930], the absence of a clear trend in the upper 50 m is common and characteristic of heterogeneous sediments made of sandy and clayey sediments [*Bartetzko and Kopf*, 2007]. Mean values and uncertainties for each site are compiled in Table 2.

[17] The density and average concentration of K, Th and U between depths of 86 m and 178 m at U1395 and between 80 m and 181 m at U1399 are tabulated in Table 3. These concentrations can be converted (equation (A5) in Appendix A) to a volumetric heat production rate of 0.257 μW/m^3 and 0.506 μW/m^3, respectively. These values are about one third and two thirds of the values for marine sediments in the Gulf of Mexico further to the west [*Nagihara et al.*, 1996]. Low heat production is likely caused by dilution with less radiogenic andesitic and mafic igneous materials in ash layers and volcaniclastic turbidites [e.g., *Plank and Langmuir*, 1998].

5. Calculation of Heat Flow

[18] To relate the near-surface temperature gradient to the heat flow from the deeper crust, the confounding (and sometimes compounding) effects of erosion, sedimentation, fluid flow, and time-varying ocean temperatures need to be assessed.

5.1. Effects of Rapid Deposition and Erosion Events

[19] The linearity of the temperature profiles in Figure 2 suggests that rapid deposition and erosion events do not dominate the present-day temperature gradient. Based on the model of thermal perturbations

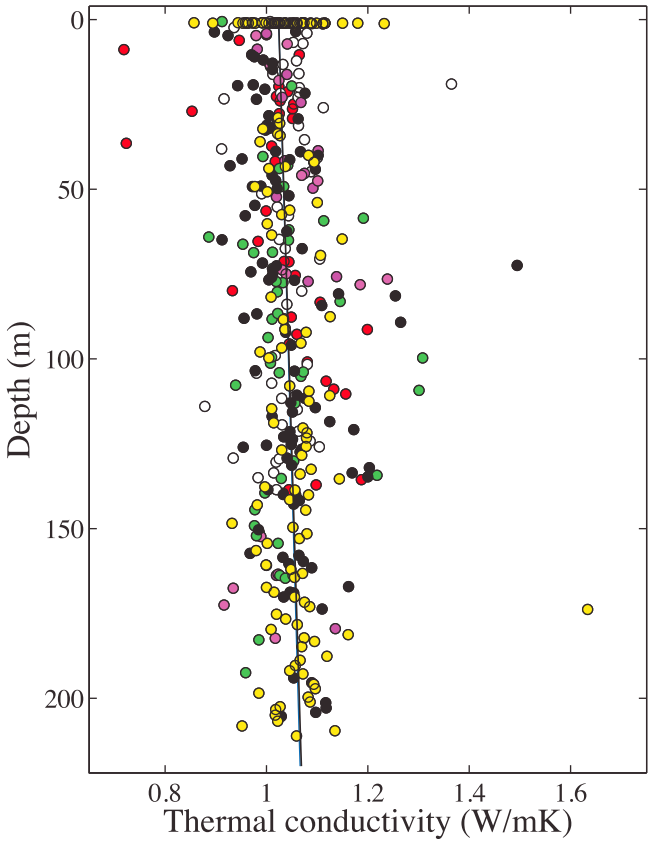

Figure 3. Thermal conductivity data. A best fit (plotted) to all the data gives $k = 1.024(\pm 0.007) + 0.00020(\pm 0.00006)$ z W/mK, where z is in m. Colors: red (U1395); white (U1396); magenta (U1397); green (U1398); black (U1399); yellow (U1400).

by unroofing events (analogous to rapid deposition events) in *Harris et al.* [2011], deposits thinner than tens of m and older than 10^4 years will have a small effect. The large debris avalanche deposit (deposit 2) mapped beneath the recovered core at Site U1395 is old enough (112–130 ka) [*Le Friant et al.*, 2004; *Lebas et al.*, 2011; *Watt et al.*, 2012] that its thermal effects will be small. A series of mass flow deposits have been emplaced in the last 14 ka in the vicinity of Site U1395 offshore Montserrat, and some of these mass flow deposits may have been hot when emplaced [*Trofimovs et al.*, 2006, 2010]. The thickest deposit (up to ~3 m) near Site U1395 was a mixed bioclastic-volcaniclastic mass flow deposit emplaced at 14 ka. This deposit may thicken markedly closer to the volcano. Mass flow deposits that are 50–100 cm thick were then emplaced at ~2 ka and 6 ka [*Trofimovs et al.*, 2006]. The ongoing eruption since 1995 has emplaced a near-surface set of stacked turbidites that are up to ~40 cm thick near Sites U1395, which are equivalent to mass flow deposits that are tens of meters thick nearer to the volcano [*Trofimovs et al.*, 2006, 2010; *Le Friant et al.*, 2008, 2010]. Individual

Table 2. Thermal Conductivity Measurements

Site	Number of Measurements	Mean	Standard Deviation	Standard Error of Mean
U1395	36	1.029 W/mK	0.100 W/mK	0.017 W/mK
U1396	50	1.041 W/mK	0.079 W/mK	0.010 W/mK
U1397	33	1.028 W/mK	0.127 W/mK	0.022 W/mK
U1398	51	1.034 W/mK	0.086 W/mK	0.012 W/mK
U1399	103	1.045 W/mK	0.080 W/mK	0.008 W/mK
U1400	161	1.050 W/mK	0.075 W/mK	0.006 W/mK

Table 3. Concentration of Heat Producing Elements Measured by Downhole Logging

Site	Depth Interval	K (%)	Th (ppm)	U (ppm)	Mean Density	Heat Production
U1395	86–178 m	0.414 ± 0.111	1.59 ± 0.66	0.936 ± 0.208	1.78 g/cm^3	0.257 μW/m^3
U1399	80–181 m	1.015 ± 0.152	5.19 ± 1.75	1.22 ± 0.42	not measured	0.506 μW/m^3

turbidites and other mass-wasting deposits identified in holes at the other sites are usually thinner than tens of meters, and the few thicker ones are older than 10^4 years old.

[20] In sum, all mass flow deposits are either thin enough, or old enough, that a thermal signature is not expected [*Harris et al.*, 2011], and none is seen in our data.

5.2. Time Varying Ocean Temperatures

[21] Intermediate and ocean bottom water temperatures vary over glacial and annual time scales by up to a degree or two [*Melling*, 1998; *Dmitrenko et al.*, 2006; *Lynch-Stieglitz et al.*, 2011]. Surface temperature perturbations with these time scales will affect subsurface temperatures to depths greater than 100 m. No evidence of this effect is seen in the curvature of the temperature profiles, but its magnitude may be too small to be identified with our low-resolution sampling.

5.3. Influence of Advection

[22] The lack of curvature (both apparent, Figure 2, and statistically except at Site U1398) in the temperature measurements in the upper 100 m argues against vertical fluid flow great enough to bias heat flow measurements. Comparison with analytical models for advective heat transport [*Bredehoeft and Papadopulos*, 1965] implies upward fluid velocities less than 10^{-10} m/s [*Ingebritsen et al.*, 2006]. At none of the sites were depth variations in pore water chemistry attributed to fluid flow [*Expedition 340 Scientists*, 2012]. Because chemical diffusivities are much smaller than thermal diffusivities, the vertical fluid velocities may thus be much smaller than the upper bound we infer from the temperature measurements.

[23] A linear increase in temperature with depth does not mean that the observed temperature is unaffected by fluid flow. Advection in permeable layers, deeper than depths at which temperature is measured, can increase [*Ziagos and Blackwell*, 1986] or decrease [*Brumm et al.*, 2009] the apparent heat flow while still maintaining a constant temperature gradient near the surface where temperature is measured. At Site U1397, there are very coarse, thick (up to ten meters) turbidite units below the depths at which temperature could be measured. Coarse turbidites less than 1 m thick are observed at all sites. Their high permeability should permit fluid advection if large enough hydraulic head gradients are generated.

[24] The role of horizontal advection is more difficult to assess without a greater density of holes at each site. Measurements at site U1399, however, suggest that horizontal fluid flow does not affect temperature. At this site the two holes were 420 m apart. Correlation of physical properties and lithology shows that there are vertical offsets up to 15 m, including the coarse turbidite units that would be the conduits for horizontal fluid flow. The temperature measurements in both holes fall on the same line, with no offset in temperature corresponding to offset in the depth of potential aquifers. The implication is that any fluid advection in permeable units does not affect the temperature distribution.

[25] On the basis of a limited data set of water column ^{3}He and Zn measurements, *Polyak et al.* [1992] suggested that there is submarine geothermal activity in the vicinity of the Kahouanne basin between Montserrat and Guadeloupe. This study has, in turn, been used to suggest that the putative hydrothermal activity is the source of the abundant ferromanganese deposits in the area [*Frank et al.*, 2006]. Our measurements, though limited to a small number of sites, find no evidence of the thermal anomalies required to sustain hydrothermal activity. Instead, our data are consistent with recent studies that suggest that the source of Fe and Mn in the ferromanganese deposits is from the low-temperature, suboxic diagenesis of freshly deposited volcanic material in the upper few cm of the sediment column [*Homoky et al.*, 2011; *Hembury et al.*, 2012].

5.4. Effects of Sediment Accumulation

[26] The accumulation of sediment on the seafloor moves isotherms downward and will suppress conductive surface heat flow relative to that at depths greater than those sampled in our holes. Estimated

sedimentation rates at each site are listed in Table 1. The average long-term sedimentation rate at Site U1395 is 90 m/Ma based on identification of the 0.99 Ma Jaramillo Matuyama reversal [*Cande and Kent*, 1995] at 90 mbsf and the first appearance of *Gephyrocapsa oceanica* (1.65 Ma) [*Kameo and Bralower*, 2000]. *Trofimovs et al.* [2006] use detailed radiocarbon dates to show sediment accumulation rates of ~140 m/Ma during the last 14 ka near Site U1395. Drilling at Site U1396 reached depths of 135 m and an age of ~4.5 Ma based on identification of the end of chron C3n.2n and Biozones CN11 (nannofossils) and PL1 (planktic foraminifera). Sedimentation rates at Site U1396 increase from about 17 m/Ma in the upper few tens of meters to roughly 53 m/Ma at 135 m [*Expedition 340 Scientists*, 2012]. At the remaining sites sedimentation rates may be as high as 500 m/Ma in the upper few hundred meters based on the presence of *Globgerinella calida* (0.22 Ma) [*Wade et al.*, 2011] and *Emiliania huxleyi* (0.25 Ma) [*Kameo and Bralower*, 2000]. Shipboard biostratigraphy and paleomagnetic interpretations are uncertain at these sites owing to prolific reworking and mixing within the debris deposits that comprise the cored sediment. We thus adopt previously published estimates of sedimentation rates in the Grenada basin that range from 40 to 200 m/Ma [*Sigurdsson et al.*, 1980; *Reid et al.*, 1996], noting that local rates may be higher or lower.

[27] To account for the effects of sedimentation, we follow *Hutchison* [1985] and compare the surface heat flow that would be measured for various sedimentation rates with that for a reference state. Briefly, we assume an initial period during which sediment accumulates at a rate of 30 m/Ma over a period of 120 Ma, a representative age for the subducting lithosphere. This reference state allows us to estimate an upper bound on the effects of sedimentation. We use a heat production rate in the surface sediment equal to the measured values of 0.257 $\mu W/m^3$ and 0.503 $\mu W/m^3$ (section 4). We assume porosity decreases exponentially with depth with an e-folding distance of 2 km. Surface porosity is 0.6 and once it decreases to 0.1 we assume no further compaction. Density, thermal conductivity, heat production, fluid and solid velocity, all vary with depth owing to compaction (see Appendix A for details). The error in the sedimentation rate correction owing to uncertainty in the various model parameters (except sedimentation rate and heat production) is less than the magnitude of the correction [*Hutchison*, 1985; *Wang and Davis*, 1992; *Hutnak and Fisher*, 2007]. To account for the effects of enhanced sedimentation that accompanies the formation of the arc, we begin with this initial condition and then continue to add sediment with a specified accumulation rate at the surface. We then compute the evolution of surface heat flow relative to that at depth. The difference between these two values approximates the underestimate based on near-surface measurements. Given the history of volcanism in the Lesser Antilles arc (section 2) we consider the influence of sedimentation over a 20 Ma period. Heat flow corrections typically level off at about 10 Ma and then gradually decrease as increased heat production, caused by sediment accumulation, counteracts advection. For sedimentation rates up to 500 m/Ma, heat flow can be underestimated by up to 10%. For our estimates of sedimentation rates (Table 1), the corrections are up to 4%, but in some cases may be less than 1%. Equations, model parameters and detailed results are included in Appendix A. Note that the sedimentation corrections in Table 1 are upper bounds given the low sedimentation rate assumed for the initial conditions and choosing the largest correction possible (Appendix A). We also neglect the effects of emplacement of hot mass flows.

5.5. Effects of Bathymetry

[28] If the seafloor is flat, we can calculate heat flow from our temperature measurements and the one-dimensional (1D) heat conduction equation. At several sites where we measured temperature, however, there is significant seafloor bathymetry with local variations in relief that can exceed 100 m. Variations in bathymetry can alter the surface heat flow relative to that at depth by up to several percent [e.g., *Blackwell et al.*, 1980]. Cold ocean water surrounds bathymetric highs. Measuring temperature at bathymetric highs, as we did at Sites U1396 and U1397, and inferring heat flow using a 1D model will therefore provide an estimate that is too low. Similarly, bathymetric lows are surrounded by sediment that is warmer than ocean water. At these sites, we will over predict heat flow if we use a 1D model. To correct for the effects of bathymetry on heat flow, we use a 3D implicit finite difference model to calculate conductive heat flow, accounting for both bathymetry and ocean temperature variations with depth. We compare the difference in temperature gradient between the 3D model and the 1D model to determine the error associated with bathymetry, and the correction that must be applied at each site. Further details are provided in Appendix B.

Table 4. Heat Flow

Site	dT/dz (K/km)	Uncorrected Heat Flow	Sedimentation Rate Correction	Bathymetry Correction
U1395	98.2 ± 8.8	0.101 ± 0.09 W/m^2	<+1%	0
U1396	69.3 ± 1.5	0.072 ± 0.02 W/m^2	<+1%	+2%
U1397	70.0 ± 8.8	0.072 ± 0.09 W/m^2	<+4%	+4%
U1398	57.4 ± 5.1	0.059 ± 0.05 W/m^2	<+4%	0
U1399	65.4 ± 0.9	0.068 ± 0.01 W/m^2	<+4%	0
U1400	52.9 ± 1.6	0.056 ± 0.04 W/m^2	<+4%	+2%

5.6. Computed Heat Flow

[29] Table 4 summarizes the measured temperature gradients, computed heat flows, and the corrections to these heat flows for the different sites. To calculate the uncorrected heat flow we multiply the average measured thermal conductivity by the measured temperature gradient. We do not evaluate the heat flow from a regression of temperature versus cumulative thermal resistance [e.g., *Bullard*, 1954] because there is no clear and significant change in k over the depth intervals that we measured temperature. The primary limitation of our heat flow values is that they are based on measurements in the upper 50–110 m and, therefore, we cannot assess the possible influence of deeper, regional fluid flow. However, we view our data as a major improvement over the majority of previous measurements in this region that were mostly based on temperature measurements in the upper few m of the seafloor [*Langseth and Grim*, 1964; *Nason and Lee*, 1964; *Vacquier and von Herzen*, 1964; *Langseth et al.*, 1966; *Epp et al.*, 1970; *Clark et al.*, 1978]. Further, we emphasize that we see no evidence in the temperature measurements for advective disturbance.

6. Comparison With Previous Measurements and Other Arcs

[30] There are few measurements that characterize the distribution of heat flow across ocean island arcs. Here we first compare our measurements with those elsewhere in and near the Lesser Antilles arc and then compare the Lesser Antilles arc with other arcs.

[31] Figure 4a shows our heat flow measurements on a cross section of the Lesser Antilles arc. We extend the cross section from the trench and across the Aves ridge. We also plot all other published heat flow measurements from this region. These other sources include measurements from ODP Leg 110 made east of the arc, near the toe of the Barbados accretionary complex [*Fisher and Hounslow*, 1990]. From this cruise, we include only estimates that include temperature measurements deeper than 50 mbsf and are not thought to be influenced by advection [*Fisher and Hounslow*, 1990]. We also include measurements reported in *Langseth and Grim* [1964], *Nason and Lee* [1964], *Vacquier and von Herzen* [1964], *Langseth et al.* [1966], *Epp et al.* [1970], and *Clark et al.* [1978]; all these studies are based on measurements made within the upper 1 to 14 m of the seafloor and reported heat flows were not corrected for the effects of sedimentation and bathymetry. We did not make such corrections to measurements from previous studies.

[32] The highest heat flow is confined to a distance less than 15 km from the axis of the arc. This is consistent with the width of intruded Lesser Antilles arc being ~25 km [*Aitken et al.*, 2011] and Pleistocene and younger magmatic activity being focused in a band less than 10 km wide in the study area [*Macdonald et al.*, 2000].

[33] Overall, our measurements are consistent with the pattern and magnitude of heat flow measured in previous studies. The lone exception is the study of *Clark et al.* [1978]. Their measurements were based on probes that penetrated between 1.2 and 3.6 m and recorded only 2 or 3 temperature measurements. In addition, *Clark et al.* [1978] did not measure ocean temperature. To the east of the Lesser Antilles arc, *Fisher and Hounslow* [1990] measured high near-surface temperature gradients that were much reduced at greater depth and attributed the steepening of shallow temperature gradients to advection. *Epp et al.* [1970] list several other reasons why shallow temperature gradients are elevated over values from deeper holes. One process they cite is compaction of very porous sediment in the upper several meters to expel enough pore water to advectively disturb shallow temperature gradients; *Bethke* [1985], however, has shown that the thermal effects of compaction are very small. We speculate that advective disturbance may be transient and

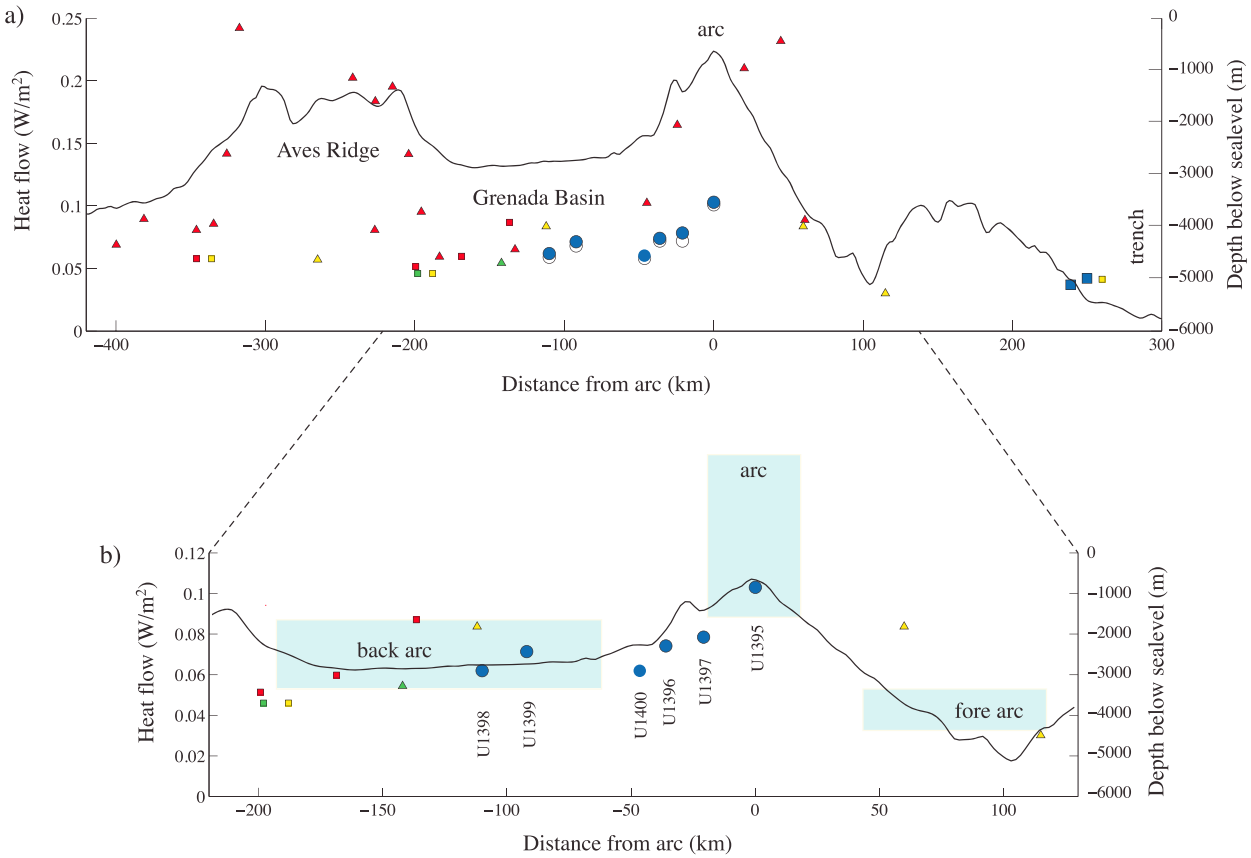

Figure 4. Cross section along line AA′ in Figure 1 showing heat flow data as a function of distance to the arc. Black curves show bathymetry along this line, with scale on the right. Measurements at U1395 and U1396 are from north of this cross section (Figure 1). (a) All data. Our measurements are shown in white, with corrected values (upper bound) in blue. Data from previous studies: red triangles [*Clark et al.*, 1978]; yellow triangles [*Vacquier and von Herzen*, 1964]; green triangles [*Nason and Lee*, 1964]; yellow squares [*Langseth et al.*, 1966]; green squares [*Langseth and Grim*, 1964]; red squares [*Epp et al.*, 1970]; blue squares [*Fisher and Hounslow*, 1990]. (b) Measurements from *Clark et al.* [1978] removed. Only upper value for our corrected heat flow is shown in Figure 4b. Notice change in scale for heat flow between Figures 4a and 4b (left axis). Also shown are typical heat flows in the fore arc, arc, and back arc.

induced by large regional earthquakes. *Wang et al.* [2012] have shown that earthquakes can change the temperature of groundwater by a degree, enough to affect inferred heat flow over periods of decades to centuries; however, changes within the upper few meters would not persist for more than decades. Deep ocean temperature in the Caribbean has also been increasing since the 1970s, by about 0.01°C/decade [*Johnson and Purkey*, 2009]. This is a small change in temperature, and would act to decrease near surface heat flow. A more plausible large source of error may be caused by small fluctuations in ocean bottom temperature, a possibility raised by *Clark et al.* [1978]. Seasonal temperature fluctuations in bottom water temperatures of >0.3°C at depths of 5 km off Barbados (to the east of the study area) lead to time varying perturbations in temperature gradients at 1 m that can exceed 50 °C/km [*Davis et al.*, 2003], comparable to the background heat flow. Large seasonal variations in heat transport through passages between the Lesser Antilles islands [e.g., *Rhein et al.*, 2005] may induce larger amplitude variations in temperature; *Clark et al.* [1978] measured heat flow in winter, and shallow temperature gradients will be enhanced by such seasonal changes in ocean-bottom temperature. Overall, we downplay the significance of the *Clark et al.* [1978] measurements because they are based on very shallow measurements of 2 or 3 temperatures, and deeper holes in this region find greatly enhanced temperature gradients at such shallow depths. In summary, we propose that our data (and other data based on more or deeper measurements)

are the most reliable and provide a consistent image of the regional heat flow.

[34] In Figure 4b we replot all the data except for those of *Clark et al.* [1978]. Once we exclude these data, there is no longer a clear distinction between the Aves ridge and the Grenada basin. Hence we cannot use a difference in heat flow to address the different origin of the crust under the northern and southern Antilles arc. Where active spreading occurs in oceanic island back arc basins, such as the Mariana marginal basin, there is a large and distinct heat flow signature [*Anderson*, 1975]. The heat flow in the Grenada basin, in contrast, is similar to typical values for oceanic crust older than about 40–50 Ma [e.g., *Parsons and Sclater*, 1977; *Stein and Stein*, 1992; *McKenzie et al.*, 2005]. The absence of a heat flow anomaly is consistent with extension in the Grenada basin having ended before 40 Ma [*Bouysse et al.*, 1990]. There is no heat flow record of episodic spreading with order 10 Ma time scales that is seen in back arcs of other oceanic island arcs [e.g., *Fackler-Adams and Busby*, 1998].

[35] Figure 4b shows the range of typical heat flows at other arcs, including the Cascades [e.g., *Ingebritsen et al.*, 1989; *Blackwell et al.*, 1990], Andes [e.g., *Henry and Pollack*, 1988; *Springer and Forster*, 1998], central America [*Ziagos et al.*, 1985], and Japan [e.g., *Furukawa et al.*, 1998]. The back arc and fore arc ranges are based on global compilations of *Currie and Hyndman* [2006] and *Stein* [2003], respectively. We do not cite all papers, selecting more recent studies and compilations that include older ones, as there are far too many to list. We do not plot the actual measurements as they are too numerous and show quite a bit of scatter. Scatter arises from two main sources: first, local variability associated with hydrothermal and shallow magmatic systems which enhance surface heat flow; second, topographically driven flow at a regional scale which acts to suppress surface heat flow [*Ingebritsen et al.*, 1989]. In fact, for both reasons it can be difficult to reliably identify temperature gradients that reflect magma and heat delivery from the mantle and mid to lower crust, leading to significant uncertainty even when deep holes are used [*Ingebritsen et al.*, 1996; *Blackwell and Priest*, 1996; *Manga*, 1998]. Instead the boxes we plot in Figure 4b capture the representative ranges for the forearc, arc, and backarc. Figure 4b shows that the Lesser Antilles does not stand out – it is a typical arc.

[36] Magma productivity over the last several Ma in the Lesser Antilles arc has been estimated to be 3–5 km^3/Ma per km of arc [*Sigurdsson et al.*, 1980; *Wadge*, 1984; *Macdonald et al.*, 2000]. These values, however, may be underestimated by a factor of about two because they neglect the mass lost in debris avalanches and other collapses [*Boudon et al.*, 2007]. For comparison, the continental Cascade Range with a similar subduction angle, subduction rate of about 3 cm/year, and comparable age, has a magma flux in the range of 10–30 km^3/Ma per km of arc [*Ingebritsen et al.*, 1989; *James et al.*, 1999]. Nevertheless, we find that the heat flow is similar, both the absolute value and its spatial variations. This is consistent with the broad, large-scale pattern of heat flow reflecting the thermal structure in the mantle wedge, which is in turn dominated by the temperature-dependence of mantle rheology [e.g., *Kelemen et al.*, 2003]. Similar heat flows at the center of most arcs (excluding locations where shallow volcanic and hydrothermal processes dominate) is consistent with its value being controlled by the depth at which magma is stored, rather than by conduction of heat from the base of the lithosphere [*Rothstein and Manning*, 2003]. The depth of protracted magma storage is controlled by the rheology and density of the crust and magma, typically 10–30 km (2–6 kbar) in continental arcs [e.g., *Zandt et al.*, 2003; *Annen et al.*, 2006]. In island arcs, magma is stored at similar pressures: in the Aleutians and Marianas, 2–5 kbar [*Baker*, 1987], and 2 kbar in the Lesser Antilles [*Martel et al.*, 1998]. In all arcs, including for example Montserrat in the Lesser Antilles [e.g., *Paulatto et al.*, 2012], there are also smaller transient storage reservoirs at shallower depths (<10 km). As there are no dramatic differences in magma storage depth and temperature, we should not expect the average heat flow to vary much from arc to arc, even when the magma flux varies by an order of magnitude. This expectation is supported by our heat flow measurements.

7. Conclusions

[37] Our measurements imply a heat flow along the crest of the active Lesser Antilles arc of about 0.10 W/m^2, similar to that at continental arcs with similar subduction rates, though with much higher magma fluxes (e.g., Cascades, USA). The region with the highest heat flow may be confined to a band that extends less than a couple tens of km from the axis of the arc, again similar to continental arcs and consistent with volcanism being confined to a narrow region. The heat flow in the center of the Grenada Basin of ~0.06 W/m^2 is consistent with both the thick crust and extension during the

Paleocene [*Bouysse et al.*, 1990]; we do not confirm the high heat flow inferred from the most recent heat flow study in the basin [*Clark et al.*, 1978].

[38] Measurements at a limited number of sites hamper our ability to draw robust, quantitative conclusions about the thermal structure and evolution of the Lesser Antilles arc from heat flow measurements. In particular we are unable to compare the young northern arc with the southern arc that has been active for over 20 Ma longer. Nonetheless, measurements from these IODP drill sites provide a high quality assessment of background heatflow across the Lesser Antilles and suggest minimal vertical fluid advection for depths shallower than ~100 mbsf along the Lesser Antilles arc and within the Grenada Basin.

Appendix A: Correction for Sedimentation

[39] Sedimentation moves cold mass downward, and hence decreases heat flow measured in shallow holes at the seafloor. As a consequence, the heat flow implied by the measured temperature gradients needs to be corrected for the history of sedimentation. Models have been used to make such corrections, and include the effects of compaction and expulsion of pore water [*Hutchison*, 1985] and additional seepage [e.g., *Hutnak and Fisher*, 2007]. Here we neglect any fluid flow except for that caused by compaction, and assume all motion and heat transfer occurs in the vertical (z) direction.

[40] Heat transfer is governed by the advection-diffusion equation

$$\overline{\rho C}\frac{\partial T}{\partial t} = \frac{\partial}{\partial z}\left[\overline{k}\frac{\partial T}{\partial z}\right] - \overline{\rho C u}\frac{\partial T}{\partial z} + \overline{A} \tag{A1}$$

where the overbar indicates bulk quantities, k is thermal conductivity, ρ is density, C is heat capacity, u is velocity (defined later in terms of sediment and fluid velocity), and A is the volumetric heat production rate.

[41] The bulk quantities in equation (A1) depend on porosity ϕ and are given by

$$\overline{\rho C} = \rho_w C_w \phi + \rho_s C_s (1-\phi) \tag{A2}$$

$$\overline{\rho C u} = \rho_w C_w \phi u_w + \rho_s C_s (1-\phi) u_s \tag{A3}$$

and

$$\overline{k} = k_w^{\phi} k_s^{1-\phi} \tag{A4}$$

where subscripts w and s denote water and sediment values, respectively. The model for thermal conductivity (A4) is adopted from previous studies of marine sediments [e.g., *Hutnak and Fisher*, 2007; *Harris et al.*, 2011] and we use k_w = 0.6 W/mK and k_s = 2.7 W/mK. We adopt ρ_s = 2800 kg/m^3 (similar to the grain density of the volcaniclastic materials we sampled), C_s = 1 kJ/kgK, and standard values for water.

[42] We calculate the heat production in units of W/m^3 from the measured concentration of K, U and Th [*Rybach*, 1988] using

$$A = 10^{-11}[\rho_w \phi + \rho_s (1-\phi)](9.52 c_U + 2.56 c_{Th} + 3.48 c_K) \tag{A5}$$

where c_U and c_{Th} are the concentrations of U and Th in ppm, respectively, and c_K is the concentration of K in weight percent.

[43] We assume that porosity decreases exponentially with depth

$$\phi(z) = \phi_0 e^{-\lambda z} \tag{A6}$$

between the surface where ϕ = 0.6 and a basement at depth $z = B$ where $\phi = \phi_B$ = 0.1. We choose the scaling depth $1/\lambda$ = 2 km.

[44] Conservation of mass for water and sediment allow us to relate u_s and u_w to ϕ,

$$\frac{d}{dz}[\rho_s u_s (1-\phi)] = 0 \tag{A7}$$

and

$$\frac{d}{dz}[\rho_s u_w \phi] = 0. \tag{A8}$$

[45] Equations (A7) and (A8) can be solved with the boundary condition that the sedimentation rate at the seafloor is u_{s0} and that at $z = B$, $u_w(z = B) = u_s(z = B)$, to give

$$u_s(z) = u_{s0}\frac{1-\phi_0}{1-\phi(z)} \tag{A9}$$

and

$$u_w(z) = u_{s0}\frac{1-\phi_0}{1-\phi_B}e^{\lambda(z-B)}. \tag{A10}$$

[46] We define B to be the depth at which ϕ = 0.1.

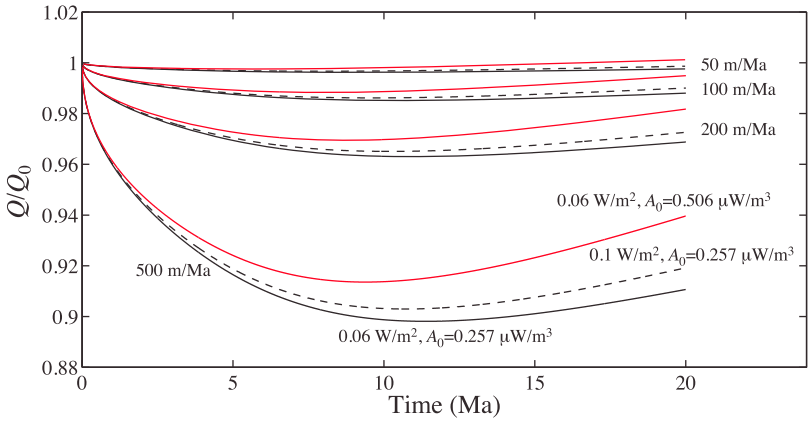

Figure A1. Near-surface heat flow (Q) relative to the heat flow at a depth of 50 km (Q_0), as a function of time. At time zero a sedimentation rate of between 50 m/Ma and 500 m/Ma is prescribed. Initial conditions and other parameters are described in the text. Background heat flow is either 0.06 W/m^2 (solid curves) or 0.1 W/m^2 (dashed curves); heat production in sediments is either 0.257 μW/m^3 (black curves) or either 0.506 μW/m^3 (red curves).

[47] We solve equation (A1) implicitly with a finite difference method. Spacing of points is 1 m. The boundary conditions on equation (A1) are $T = 0$ at $z = 0$ and at a depth of 50 km, we fix the heat flow to Q_0.

[48] We compute an initial condition by calculating a temperature distribution in the crust for a specified Q_0. We begin the evolution of this crust with depth-distribution of properties implied by equation (A6) and no heat production within the crust. We then allow sediment to accumulate at a rate of 30 m/Ma, with heat production given by (A5). The temperature distribution after 120 Ma for this case is then used as the initial condition to examine the effect of sedimentation rate. We chose this age as it represents the South American plate and is old enough that a nearly steady heat flow has been reached. We define this state as $t = 0$.

[49] Figure A1 shows the evolution of heat flow for sedimentation rates between 50 and 500 m/Ma for background heat flows of 0.06 and 0.1 W/m^2. The increase in sedimentation rate suppresses surface heat flow from a couple percent to about 10 percent over the 5 to 20 Ma period of interest. Close to steady state conditions are reached by about 10 Ma.

Appendix B: Correction for Bathymetry

[50] To calculate the effects of bathymetry on heat flow, we solve the steady heat conduction equation with a 3D implicit second-order finite difference scheme that incorporates bathymetric data at each of the drill sites. We fix thermal conductivity everywhere to 1 W/mK. The surface upper boundary condition is held constant in time but temperature varies with bathymetry. We constrain the relationship between temperature and bathymetry by averaging measurements from four Conductivity-Temperature-Depth (CTD) casts collected by Katz during research cruise RC2906 in 1988, and by Ewing on research cruise RC1510 in 1972. These data are unpublished but available from *GeoMapApp* (http://www.geomapapp.org), a data distribution site maintained by Lamont-Doherty Earth Observatory. At a depth of 1 km below the seafloor, we apply a constant heat flow of 0.05 W/m^2. We use a seafloor bathymetry with a resolution of 110 × 110 × 12.5 m in the x,y,z directions respectively [*Ryan et al.*, 2009]. Drill sites are located in the middle of each of these models to minimize the effects of all side boundary conditions. The initial conditions assume a 1D temperature profile at each of the cells. Heat flow at Sites U1396 and U1397 are most affected by bathymetry, with both sites located on bathymetric highs. The analysis indicates that measured heat flow at Site U1396 is too low by no more than 2%. Similarly, measured heat flow at Site U1397 is too low by no more than 4%. The depth at which peak differences in temperature occur between 1D and 3D models is between 50 and 80 m. At all other sites the seafloor is nearly flat, and bathymetric effects are negligible.

Acknowledgments

[51] Data and funding provided by IODP. MM received additional support from the NSF FESD program. The authors thank the remaining shipboard scientists (Daisuke Endo, James

McManus) and the outstanding technical staff for making the measurements possible. Thomas Bodin did the transdimensional regression of data from Site U1398. Comments and suggestions by R.N. Harris and reviewers are appreciated.

References

Aitken, T., P. Mann, A. Escalona, and G. L. Christeson (2011), Evolution of the Grenada and Tobago basins and implications for arc migration, *Mar. Pet. Geol.*, *28*, 235–258, doi:10.1016/j.marpetgeo.2009.10.003.

Anderson, R. N. (1975), Heat flow in the Mariana Marginal Basin, *J. Geophys. Res.*, *80*, 4043–4048, doi:10.1029/JB080i029p04043.

Annen, C., J. D. Blundy, and R. S. J. Sparks (2006), The generation of intermediate and silicic magmas in deep crustal hot zones, *J. Petrol.*, *47*, 505–539, doi:10.1093/petrology/egi084.

Athy, L. F. (1930), Density, porosity, and compaction of sedimentary rocks, *AAPG Bull.*, *14*, 1–23.

Baker, D. R. (1987), Depths and water content of magma chambers in the Aleutian and Marianas island arcs, *Geology*, *15*, 496–499, doi:10.1130/0091-7613(1987)15<496:DAWCOM>2.0.CO;2.

Bartetzko, A., and A. K. Kopf (2007), The relationship of undrained shear strength and porosity with depth in shallow (<50 m) marine sediments, *Sediment. Geol.*, *196*, 235–249, doi:10.1016/j.sedgeo.2006.04.005.

Bethke, C. (1985), A numerical model of compaction-driven groundwater flow and heat transfer and its application to paleohydrology of intracratonic sedimentary basins, *J. Geophys. Res.*, *90*, 6817–6828, doi:10.1029/JB090iB08p06817.

Blackwell, D. D., and G. R. Priest (1996), Comment on "Rates and patterns of groundwater flow in the Cascade Range volcanic arc and the effect of subsurface temperatures" by S. E. Ingebritsen, D. R. Sherrod, and R. H. Mariner, *J. Geophys. Res.*, *101*, 17,561–17,568, doi:10.1029/96JB01507.

Blackwell, D. D., J. L. Steele, and C. A. Brott (1980), The terrain effect on terrestrial heat flow, *J. Geophys. Res.*, *85*, 4757–4772, doi:10.1029/JB085iB09p04757.

Blackwell, D. D., R. G. Bowen, D. A. Hull, J. Riccio, and J. L. Steele (1982), Heat flow, arc volcanism, and subduction in northern Oregon, *J. Geophys. Res.*, *87*, 8735–8754, doi:10.1029/JB087iB10p08735.

Blackwell, D. D., J. L. Steele, and S. Kelley (1990), Heat flow in the state of Washington and thermal conditions in the Cascade Range, *J. Geophys. Res.*, *95*, 19,495–19,516, doi:10.1029/JB095iB12p19495.

Blum, P. (1997), Physical properties handbook: A guide to the shipboard measurement of physical properties of deep-sea cores, *ODP Tech. Note*, *26*, Ocean Drill. Program, College Station, Tex.

Boudon, G., A. Le Friant, J.-C. Komorowski, C. Deplus, and M. P. Semet (2007), Volcano flank instability in the Lesser Antilles Arc: Diversity of scale, processes, and temporal recurrence, *J. Geophys. Res.*, *112*, B08205, doi:10.1029/2006JB004674.

Bouysse, P. (1988), Opening of the Grenada back-arc basin and evolution of the Caribbean plate during the Mesozoic and Paleogene, *Tectonophysics*, *149*, 121–143, doi:10.1016/0040-1951(88)90122-9.

Bouysse, P., D. Westercamp, and P. Andrieff (1990), The Lesser Antilles island arc, *Proc. Ocean Drill. Program Sci. Results*, *110*, 29–44.

Boynton, C. H., G. K. Westbrook, M. H. P. Bott, and R. E. Long (1979), A seismic refraction investigation of crustal structure beneath the Lesser Antilles island arc, *Geophys. J. R. Astron. Soc.*, *58*, 371–393, doi:10.1111/j.1365-246X.1979.tb01031.x.

Bredehoeft, J. D., and I. S. Papadopulos (1965), Rates of vertical groundwater movement estimated from the Earth's thermal profile, *Water Resour. Res.*, *1*, 325–328, doi:10.1029/WR001i002p00325.

Brumm, M., C.-Y. Wang, and M. Manga (2009), Spring temperatures in the Sagehen Basin, Sierra Nevada, California: Implications for heat flow and groundwater circulation, *Geofluids*, *9*, 195–207, doi:10.1111/j.1468-8123.2009.00254.x.

Bullard, E. C. (1954), The flow of heat through the floor of the Atlantic Ocean, *Proc. R. Soc. A*, *222*, 408–429, doi:10.1098/rspa.1954.0085.

Cande, S. C., and D. V. Kent (1995), Revised calibration of the geomagnetic polarity timescale for the Late Cretaceous and Cenozoic, *J. Geophys. Res.*, *100*, 6093–6095, doi:10.1029/94JB03098.

Clark, T. F., B. J. Korgen, and D. M. Best (1978), Heat flow in the eastern Caribbean, *J. Geophys. Res.*, *83*, 5883–5891, doi:10.1029/JB083iB12p05883.

Currie, C. A., and R. D. Hyndman (2006), The thermal structure of subduction zone back arcs, *J. Geophys. Res.*, *111*, B08404, doi:10.1029/2005JB004024.

Davies, J. H., and D. R. Davies (2010), Earth's surface heat flux, *Solid Earth*, *1*, 5–24, doi:10.5194/se-1-5-2010.

Davis, E. E., K. Wang, K. Becker, R. E. Thompson, and I. Yashayaev (2003), Deep-ocean temperature variations and implications for errors in seafloor heat flow determinations, *J. Geophys. Res.*, *108*(B1), 2034, doi:10.1029/2001JB001695.

Dmitrenko, I. A., I. V. Polyakov, S. A. Kirillov, L. A. Timokhov, H. L. Simmons, V. V. Ivanov, and D. Walsh (2006), Seasonal variability of Atlantic water on the continental slope of the Laptev Sea during 2002–2004, *Earth Planet. Sci. Lett.*, *244*, 735–743, doi:10.1016/j.epsl.2006.01.067.

England, P. C., and R. F. Katz (2010), Melting above the anhydrous solidus controls the location of volcanic arcs, *Nature*, *467*, 700–703, doi:10.1038/nature09417.

Epp, D., P. J. Grim, and M. G. Langseth (1970), Heat flow in the Caribbean and Gulf of Mexico, *J. Geophys. Res.*, *75*, 5655–5669, doi:10.1029/JB075i029p05655.

Expedition 340 Scientists (2012), Lesser Antilles volcanism and landslides: Implications for hazard assessment and long-term magmatic evolution of the arc, *Integrated Ocean Drill. Program Prelim. Rep.*, *340*, doi:10.2204/iodp.pr.340.2012.

Fackler-Adams, B. N., and C. J. Busby (1998), Structural and stratigraphic evolution of extensional oceanic arcs, *Geology*, *26*, 735–738, doi:10.1130/0091-7613(1998)026<0735:SASEOE>2.3.CO;2.

Fisher, A. T., and M. W. Hounslow (1990), Heat flow through the toe of the Barbados accretionary complex, *Proc. Ocean Drill. Program Sci. Results*, *110*, 345–363.

Fisher, A. T., H. Villinger, and M. Heesemann (2007), User manual for the third-generation, advanced piston corer temperature tool (APCT-3), 42 pp., Integrated Ocean Drill. Program, College Station, Tex.

Frank, M., H. Marbler, A. Koschinsky, T. van de Flierdt, V. Klemm, M. Gutjahr, A. N. Halliday, P. W. Kubik, and P. Halbach (2006), Submarine hydrothermal venting related to volcanism in the Lesser Antilles: Evidence from ferromanganese precipitates, *Geochem. Geophys. Geosyst.*, *7*, Q04010, doi:10.1029/2005GC001140.

Furukawa, Y. (1993), Depth of the decoupling plate interface and thermal structure under arcs, *J. Geophys. Res.*, *98*, 20,005–20,013, doi:10.1029/93JB02020.

Furukawa, Y., H. Shinjoe, and S. Nishimura (1998), Heat flow in the southwest Japan arc and its implication for thermal processes under arcs, *Geophys. Res. Lett.*, *25*, 1087–1090, doi:10.1029/98GL00545.

Gallagher, K., T. Bodin, M. Sambridge, D. Weiss, M. Kylander, and D. Large (2011), Inference of abrupt changes in noisy geochemical records using transdimensional changepoint models, *Earth Planet. Sci. Lett.*, *311*, 182–194, doi:10.1016/j.epsl.2011.09.015.

Germa, A., X. Quidelleur, S. Labanieh, C. Chauval, and P. Lahitte (2011), The volcanic evolution of Martinique Island: Insights from K-Ar dating into the Lesser Antilles arc migration since the Oligocene, *J. Volcanol. Geotherm. Res.*, *208*, 122–135, doi:10.1016/j.jvolgeores.2011.09.007.

Harford, C. L., M. S. Pringle, R. S. J. Sparks, and S. R. Young (2002), The volcanic evolution of Montserrat using $^{40}Ar/^{39}Ar$ geochronology, in *The Eruption of Soufriere Hills Volcano, Montserrat From 1995 to 1999*, edited by T. H. Druitt and B. P. Kokelaar, *Mem. Geol. Soc. London*, *21*, 93–113.

Harris, R. N., F. Schmidt-Schierhorn, and G. Spinelli (2011), Heat flow along the NanTroSEIZE transect: Results from IODP Expeditions 315 and 316 offshore the Kii Peninsula, Japan, *Geochem. Geophys. Geosyst.*, *12*, Q0AD16, doi:10.1029/2011GC003593.

Heesemann, M., H. Villinger, A. T. Fisher, A. M. Trehu, and S. White (2006), Data report: Testing and deployment of the new APCT-3 tool to determine in situ temperatures while piston coring, *Proc. Integrated Ocean Drill. Program*, *311*, 1–19, doi:10.2204/iodp.proc.311.108.2006.

Hembury, D. J., M. R. Palmer, G. R. Fones, R. A. Mills, R. Marsh, and M. T. Jones (2012), Uptake of dissolved oxygen during marine diagenesis of fresh volcanic material, *Geochim. Cosmochim. Acta*, *84*, 353–368, doi:10.1016/j.gca.2012.01.017.

Henry, S. G., and H. N. Pollack (1988), Terrestrial heat flow above the Andean subduction zone in Bolivia and Peru, *J. Geophys. Res.*, *93*, 15,153–15,162, doi:10.1029/JB093iB12p15153.

Homoky, W. B., D. J. Hembury, L. E. Hepburn, R. A. Mills, P. J. Statham, G. R. Fones, and M. R. Palmer (2011), Iron and manganese diagenesis in deep sea volcanogenic sediments and the origins of pore water colloids, *Geochim. Cosmochim. Acta*, *75*, 5032–5048, doi:10.1016/j.gca.2011.06.019.

Hutchison, I. (1985), The effects of sedimentation and compaction on oceanic heat flow, *Geophys. J. R. Astron. Soc.*, *82*, 439–459, doi:10.1111/j.1365-246X.1985.tb05145.x.

Hutnak, M., and A. T. Fisher (2007), Influence of sedimentation, local and regional hydrothermal circulation, and thermal rebound on measurements of seafloor heat flux, *J. Geophys. Res.*, *112*, B12101, doi:10.1029/2007JB005022.

Ingebritsen, S. E., D. R. Sherrod, and R. H. Mariner (1989), Heat flow and hydrothermal circulation in the Cascade Range, north-central Oregon, *Science*, *243*, 1458–1462, doi:10.1126/science.243.4897.1458.

Ingebritsen, S. E., D. R. Sherrod, and R. H. Mariner (1996), Reply to comment on "Rates and pattern of groundwater flow in the Cascade Range volcanic arc, and the effect on subsurface temperatures," *J. Geophys. Res.*, *101*, 17,569–17,576, doi:10.1029/96JB01506.

Ingebritsen, S., W. Sanford, and C. Neuzil (2006), *Groundwater in Geologic Processes*, Cambridge Univ. Press, New York.

James, E. R., M. Manga, and T. P. Rose (1999), CO_2 degassing in the Oregon Cascades, *Geology*, *27*, 823–826, doi:10.1130/0091-7613(1999)027<0823:CDITOC>2.3.CO;2.

Jaupart, C., and J.-C. Mareschal (2011), *Heat Generation and Transport in the Earth*, Cambridge Univ. Press, New York.

Johnson, G. C., and S. G. Purkey (2009), Deep Caribbean Sea warming, *Deep Sea Res.*, Part I, *56*, 827–834, doi:10.1016/j.dsr.2008.12.011.

Kameo, K., and T. J. Bralower (2000), Neogene calcareous nannofossil biostratigraphy of sites 998, 999, ad 1000, Caribbean Sea, *Proc. Ocean Drill. Program Sci. Results*, *165*, 3–17.

Keenan, J. H., F. G. Keyes, P. G. Hill, and J. G. Moore (1978), *Steam Tables: Thermodynamic Properties of Water Including Vapor, Liquid and Solid Phases*, John Wiley, New York.

Kelemen, P. B., J. L. Rilling, E. M. Parmentier, L. Mehl, and B. R. Hacker (2003), Thermal structure due to solid-state flow in the mantle wedge beneath arcs, in *Inside the Subduction Factory*, *Geophys. Monogr. Ser.*, vol. 138, edited by J. Eiler, pp. 293–311, AGU, Washington, D. C., doi:10.1029/138GM13.

Kopp, H., et al. (2011), Deep structure of the central Lesser Antiles Island Arc: Relevance for the formation of continental crust, *Earth Planet. Sci. Lett.*, *304*, 121–134, doi:10.1016/j.epsl.2011.01.024.

Langseth, M. G., and P. J. Grim (1964), New heat-flow measurements in the Caribbean and western Atlantic, *J. Geophys. Res.*, *69*, 4916–4917, doi:10.1029/JZ069i022p04916.

Langseth, M. G., X. LePichon, and M. Ewing (1966), Crustal structure of the mid-ocean ridges: 5. Heat flow through the Atlantic Ocean floor and convection currents, *J. Geophys. Res.*, *71*, 5321–5355, doi:10.1029/JZ071i022p05321.

Lavoie, D. L., T. R. Bruns, and K. M. Fischer (1994), Geotechnical and logging evidence for underconsolidation of Lau Basin sediments: Rapid sedimentation vs. fluid flow, *Proc. Ocean Drill. Program Sci. Results*, *135*, 787–795.

Lebas, E., A. Le, G. Friant, S. F. L. Boudon, P. J. Watt, N. Talling, C. Feuillet, C. Deplus, C. Berndt, and M. Vardy (2011), Multiple widespread landslides during the long-term evolution of a volcanic island: Insights from high-resolution seismic data, Montserrat, Lesser Antilles, *Geochem. Geophys. Geosyst.*, *12*, Q05006, doi:10.1029/2010GC003451.

Le Friant, A., C. Harford, C. Deplus, G. Boudon, R. S. J. Sparks, R. Herd, and J.-C. Komorowski (2004), Geomorphological evolution of Montserrat (West Indies): Importance of flank collapse and erosional processes, *J. Geol. Soc.*, *161*, 147–160, doi:10.1144/0016-764903-017.

Le Friant, A., E. J. Locke, M. B. Hart, M. J. Leng, C. W. Smart, R. S. J. Sparks, G. Boudon, C. Deplus, and J.-C. Komorowski (2008), Late Pleistocene tephrachronology of marine sediments adjacent to Monserrat, Lesser Antilles volcanic arc, *J. Geol. Soc.*, *165*, 279–289, doi:10.1144/0016-76492007-019.

Le Friant, A., et al. (2010), The eruption of Soufrière Hills (1995–2009) from an offshore perspective: Insights from repeated swath bathymetry surveys, *Geophys. Res. Lett.*, *37*, L11307, doi:10.1029/2010GL043580.

Lynch-Stieglitz, J., M. W. Schmidt, and W. B. Curry (2011), Evidence from the Florida Straits for Younger Dryas ocean circulation changes, *Paleoceanography*, *26*, PA1205, doi:10.1029/2010PA002032.

Macdonald, K. C., and T. L. Holcombe (1978), Investigations of magnetic anomalies and sea floor spreading in the Cayman Trough, *Earth Planet. Sci. Lett.*, *40*, 407–414, doi:10.1016/0012-821X(78)90163-2.

Macdonald, R., C. J. Hawkesworth, and E. Heath (2000), The Lesser Antilles volcanic chain: A study in arc magmatism,

Earth Sci. Rev., *49*, 1–76, doi:10.1016/S0012-8252(99)00069-0.

Manga, M. (1998), Advective heat transport by low temperature discharge in the Oregon Cascades, *Geology*, *26*, 799–802, doi:10.1130/0091-7613(1998)026<0799:AHTBLT>2.3.CO;2.

Martel, C., M. Pichavant, J.-L. Bourdier, H. Traineau, F. Holt, and B. Scaillet (1998), Magma storage conditions and control of eruption regime in silicic volcanoes: Experimental evidence from Mt. Pelee, *Earth Planet. Sci. Lett.*, *156*, 89–99, doi:10.1016/S0012-821X(98)00003-X.

McKenzie, D., J. Jackson, and K. Priestley (2005), Thermal structure of oceanic and continental lithosphere, *Earth Planet. Sci. Lett.*, *233*, 337–349, doi:10.1016/j.epsl.2005.02.005.

Melling, H. (1998), Hydrographic changes in the Canada Basin of the Arctic Ocean, 1979–1996, *J. Geophys. Res.*, *103*, 7637–7645, doi:10.1029/97JC03723.

Minster, J. B., and T. H. Jordan (1978), Present-day plate motions, *J. Geophys. Res.*, *83*, 5331–5354, doi:10.1029/JB083iB11p05331.

Nagihara, S., J. G. Sclater, J. D. Phillips, E. W. Behrens, T. Lewis, L. A. Lawyer, Y. Nakamura, J. Garcia-Abdeslem, and A. Maxwell (1996), Heat flow in the western abyssal plain of the Gulf of Mexico: Implications for thermal evolution of the old oceanic lithosphere, *J. Geophys. Res.*, *101*, 2895–2913, doi:10.1029/95JB03450.

Nason, R. D., and W. H. K. Lee (1964), Heat-flow measurements in the North Atlantic, Caribbean, and Mediterranean, *J. Geophys. Res.*, *69*, 4875–4883, doi:10.1029/JZ069i022p04875.

Neill, I., A. C. Kerr, A. R. Hastie, K.-P. Stanek, and I. L. Millar (2011), Origin of the Aves ridge and Dutch-Venezuelan Antilles: Interaction of the Cretaceous 'Great Arc' and Caribbean-Colombian oceanic plateau?, *J. Geol. Soc.*, *168*, 333–348, doi:10.1144/0016-76492010-067.

Parson, L., J. Hawkins, J. Allan, and the Leg 135 Science Party (1992), *Proceedings of the Ocean Drilling Program: Initial Reports*, vol. 135, Ocean Drill. Program, College Station, Tex.

Parsons, B., and J. G. Sclater (1977), An analysis of the variation of the ocean floor bathymetry and heat flow with age, *J. Geophys. Res.*, *82*, 803–827, doi:10.1029/JB082i005p00803.

Paulatto, M., C. Annen, T. J. Henstock, E. Kiddle, T. A. Minshull, R. S. J. Sparks, and B. Voight (2012), Magma chamber properties from integrated seismic tomography and thermal modeling at Montserrat, *Geochem. Geophys. Geosyst.*, *13*, Q01014, doi:10.1029/2011GC003892.

Plank, T., and C. H. Langmuir (1988), An evaluation of the global variations in the major element chemistry of arc basalts, *Earth Planet. Sci. Lett.*, *90*, 349–370, doi:10.1016/0012-821X(88)90135-5.

Plank, T., and C. H. Langmuir (1998), The chemical composition of subducting sediment and its consequences for the crust and mantle, *Chem. Geol.*, *145*, 325–394, doi:10.1016/S0009-2541(97)00150-2.

Pollack, H. N., S. J. Hurter, and J. R. Johnson (1993), Heat flow from the Earth's interior: Analysis of the global data set, *Rev. Geophys.*, *31*, 267–280, doi:10.1029/93RG01249.

Polyak, B. G., et al. (1992), Evidence of submarine hydrothermal discharge to the northwest of Guadeloupe Island (Lesser Antilles island arc), *J. Volcanol. Geotherm. Res.*, *54*, 81–105, doi:10.1016/0377-0273(92)90116-U.

Porritt, R. W., R. M. Allen, D. C. Boyarko, and M. R. Brudzinski (2011), Investigation of Cascadia segmentation with ambient noise tomography, *Earth Planet. Sci. Lett.*, *309*, 67–76, doi:10.1016/j.epsl.2011.06.026.

Press, W. H., S. A. Teukolsky, W. T. Vetterling, and B. P. Flannery (1992), *Numerical Recipes: The Art of Scientific Computing*, 2nd ed., Cambridge Univ. Press, New York.

Ratcliffe, E. H. (1960), The thermal conductivities of ocean sediments, *J. Geophys. Res.*, *65*, 1535–1541, doi:10.1029/JZ065i005p01535.

Reid, R. P., S. N. Carey, and D. R. Ross (1996), Late Quaternary sedimentation in the Lesser Antilles island arc, *Geol. Soc. Am. Bull.*, *108*, 78–100, doi:10.1130/0016-7606(1996)108<0078:LQSITL>2.3.CO;2.

Rhein, M., K. Kirchner, C. Mertens, R. Steinfeldt, M. Walter, and U. Fleischmann-Wischnath (2005), Transport of south Atlantic water through the passages south of Guadeloup and across 16°N, 2000–2004, *Deep Sea Res.*, *52*, 2234–2249, doi:10.1016/j.dsr.2005.08.003.

Rothstein, D. A., and C. E. Manning (2003), Geothermal gradients in continental magmatic arcs: Constraints from the eastern Peninsular Ranges batholith, Baja California, Mexico, in *Tectonic Evolution of Northwestern Mexico and the Southwestern USA*, edited by S. E. Johnson et al., *Spec. Pap. Geol. Soc. Am.*, *375*, 337–354, doi:10.1130/0-8137-2374-4.337.

Ryan, W. B. F., et al. (2009), Global multi-resolution topography synthesis, *Geochem. Geophys. Geosyst.*, *10*, Q03014, doi:10.1029/2008GC002332.

Rybach, L. (1988), Determination of heat production rate, in *Handbook of Terrestrial Heat Flow Density Determination*, edited by R. Hanel, L. Rybach, and L. Stegna, pp. 125–142, Kluwer, Dordrecht, Netherlands.

Schellart, W. P. (2004), Kinematics of subduction and subduction-induced flow in the upper mantle, *J. Geophys. Res.*, *109*, B07401, doi:10.1029/2004JB002970.

Sclater, J. G. (1972), Heat flow and elevation of the marginal basins of the western Pacific, *J. Geophys. Res.*, *77*, 5705–5719, doi:10.1029/JB077i029p05705.

Sevilla, W. I., C. J. Ammon, B. Voight, and S. De Angelis (2010), Crustal structure beneath the Montserrat region of the Lesser Antilles island arc, *Geochem. Geophys. Geosyst.*, *11*, Q06013, doi:10.1029/2010GC003048.

Sigurdsson, H., R. S. J. Sparks, C. N. Carey, and T. C. Huang (1980), Volcanogenic sedimentation in the Lesser Antilles arc, *J. Geol.*, *88*, 523–540, doi:10.1086/628542.

Speed, R. C., and J. A. Walker (1991), Oceanic-crust of the Grenada basin in the southern Lesser Antilles arc platform, *J. Geophys. Res.*, *96*, 3835–3851, doi:10.1029/90JB02558.

Springer, M., and A. Forster (1998), Heat-flow density across the central Andean subduction zone, *Tectonophysics*, *291*, 123–139, doi:10.1016/S0040-1951(98)00035-3.

Stegman, D. R., J. Freeman, W. P. Schellart, L. Moresi, and D. May (2006), Influence of trench width on subduction hinge retreat rates in 3-D models of slab rollback, *Geochem. Geophys. Geosyst.*, *7*, Q03012, doi:10.1029/2005GC001056.

Stein, C. A. (2003), Heat flow and flexure at subduction zones, *Geophys. Res. Lett.*, *30*(23), 2197, doi:10.1029/2003GL018478.

Stein, C. A., and S. Stein (1992), A model for the global variation in oceanic depth and heat flow with lithospheric age, *Nature*, *359*, 123–129, doi:10.1038/359123a0.

Trofimovs J., et al. (2006), Submarine pyroclastic deposits formed at the Soufriere Hills volcano, Montserrat (1995–2003): What happens when pyroclastic flows enter the ocean?, *Geology*, *34*, 549–552, doi:10.1130/G22424.1.

Trofimovs, J., et al. (2010), Evidence for carbonate platform failure during rapid sea level rise; *ca* 14,000 year old bioclastic flow deposits in the Lesser Antilles, *Sedimentology*, *57*, 735–759, doi:10.1111/j.1365-3091.2009.01117.x.

Vacquier, V., and R. P. von Herzen (1964), Evidence for connection between heat flow and the mid-Atlantic ridge magnetic anomaly, *J. Geophys. Res.*, *69*, 1093–1101, doi:10.1029/JZ069i006p01093.

Wade, B., P. N. Peason, W. Berggren, and H. Pälike (2011), Review and revision of Cenozoic tropical planktonic foraminiferal biostratigraphy and calibration to the geomagnetic polarity and astronomical time scale, *Earth Sci. Rev.*, *104*, 111–142, doi:10.1016/j.earscirev.2010.09.003.

Wadge, G. (1984), Comparison of volcanic production rates and subduction rates at the Lesser Antilles and Central America, *Geology*, *12*, 555–558, doi:10.1130/0091-7613(1984)12<555:COVPRA>2.0.CO;2.

Wang, C.-Y., M. Manga, C.-H. Wang, and C.-Y. Chen (2012), Earthquakes and subsurface temperature changes near an active mountain front, *Geology*, *40*, 119–122, doi:10.1130/G32565.1.

Wang, K., and E. E. Davis (1992), Thermal effects of marine sedimentation in hydrothermally active areas, *Geophys. J. Int.*, *110*, 70–78, doi:10.1111/j.1365-246X.1992.tb00714.x.

Watt, S. F. L., et al. (2012), Emplacement dynamics and tsunami hazards from volcanic island flank collapses and adjacent seafloor sediment failures, *Earth Planet. Sci. Lett.*, *319–320*, 228–240, doi:10.1016/j.epsl.2011.11.032.

White, S. M., J. A. Crisp, and F. J. Spera (2006), Long term eruption rates and magma budgets, *Geochem. Geophys. Geosyst.*, *7*, Q03010, doi:10.1029/2005GC001002.

Yuan, X., S. V. Sobolev, and R. Kind (2002), Moho topography in the central Andes and its geodynamic implications, *Earth Planet. Sci. Lett.*, *199*, 389–402, doi:10.1016/S0012-821X(02)00589-7.

Zandt, G., M. Leidig, J. Chmielowski, D. Baumont, and X. Yuan (2003), Seismic detection and characterization of the Altiplano-Puna magma body, central Andes, *Pure Appl. Geophys.*, *160*, 789–807, doi:10.1007/PL00012557.

Zellmer, G. F. (2009), Petrogenesis of Sr-rich adakitic rocks at volcanic arcs: Insights from global variations of eruptive style with plate convergence rates and surface heat flux, *J. Geol. Soc.*, *166*, 725–734, doi:10.1144/0016-76492008-0721.

Ziagos, J. P., and D. D. Blackwell (1986), A model for the transient temperature effects of horizontal fluid flow in geothermal systems, *J. Volcanol. Geotherm. Res.*, *27*, 371–397, doi:10.1016/0377-0273(86)90021-1.

Ziagos, J. P., D. D. Blackwell, and F. Mooser (1985), Heat flow in southern Mexico and the thermal effects of subduction, *J. Geophys. Res.*, *90*, 5410–5420, doi:10.1029/JB090iB07p05410.